

ShakingAlarm: A Nontraditional Regional Earthquake Early Warning System Based on Time-Dependent Anisotropic Peak Ground-Motion Attenuation Relationships

by Benjamin Ming Yang, Ting-Chung Huang,* and Yih-Min Wu*

Abstract The *P*-alert seismic network, an on-site low-cost earthquake early warning system (EEWS) located in Taiwan, has proven useful in earthquake events since 2010. This dense network can produce detailed shakemaps and identify the direction of the source rupture in near-real time. Based on real-time acceleration signals and the proposed time-dependent anisotropic attenuation relationship with peak ground acceleration (PGA), ShakingAlarm, a regional early warning system add-on to the original *P*-alert network, can immediately provide (1) an accurate predicted PGA, before the arrival of the observed PGA, that will give a consistent lead time for hazard assessment and emergency response, (2) a predicted shakemap (PSM) that will converge faster to the final reported shakemap than the regional EEWS, and (3) a shake contour area-based magnitude estimation that is robust, even in the absence of a measured shake contour area such as in the case of an offshore earthquake. Taking the 2016 M_w 6.4 Meinong earthquake as an example, the 14th second PSM from ShakingAlarm converges on the final shakemap better than the regional EEWS from the Central Weather Bureau (CWB) in Taiwan. According to our tests, ShakingAlarm provides a warning using modified Mercalli intensity (MMI) V that is consistent with the results of another on-site EEWS (Strategies and Tools for Real Time Earthquake Risk ReducTION [REAKT]). Further performance tests were conducted with another five $M_L > 5.5$ inland earthquakes from 2013 to 2014. Compared with traditional regional EEWSs, ShakingAlarm can effectively identify possible damage regions and provide valuable early warning information (PSM, predicted PGA, and magnitude) for risk mitigation.

Introduction

Located on the western circum-Pacific seismic belt, Taiwan is frequently struck by earthquakes. The collision between the nearby Philippine Sea and Eurasian plates contributes to the complex geological features of Taiwan. To the northeast of Taiwan, the Philippine Sea plate subducts northward under the Eurasian plate along the Ryukyu trench (Wu *et al.*, 2008). At the southern tip of Taiwan, the Eurasian plate subducts eastward under the Philippine Sea plate. Tectonically, most of Taiwan is under northwest–southeast (NW–SE) compression, with a measured convergence rate of ~ 8 cm/yr (see Fig. 1). In the past, damaging earthquakes have caused many casualties. For example, in 1935, a large earthquake (M 7.1) occurred in the Hsinchu–Taichung area (3276 deaths, 12,053 injuries, 17,907 houses destroyed, and 37,781 houses damaged), and in 1999, the Chi-Chi earth-

quake (M_w 7.6) occurred in Nantou County (2456 deaths, 11,306 injuries, and 4 billion in property damage; Wu and Teng, 2002). The presence of large earthquakes in Taiwan highlights the constant need to develop better early warning systems and to improve earthquake engineering.

Since Cooper (1868) developed the concept of the earthquake early warning system (EEWS), many EEWSs have been built around the world (e.g., Nakamura, 1988; Espinosa-Aranda *et al.*, 1995; Allen, Brown, *et al.*, 2009; Allen, Gasparini *et al.*, 2009; Satriano *et al.*, 2011; Wu *et al.*, 2013; Wu, 2015; Clinton *et al.*, 2016), and these systems have played an important role in risk mitigation (Kanamori *et al.*, 1997). At present, there are two types of EEWSs, regional and on-site EEWSs.

Regional early warning systems, including that built by the Taiwan Central Weather Bureau (CWB; Wu and Teng, 2002; Hsiao *et al.*, 2009, 2011), collect real-time strong ground motion signals, determine earthquake source param-

*Also at Institute of Earth Sciences, Academia Sinica 128, Section 2, Academia Road, Nangang, Taipei 11529, Taiwan.

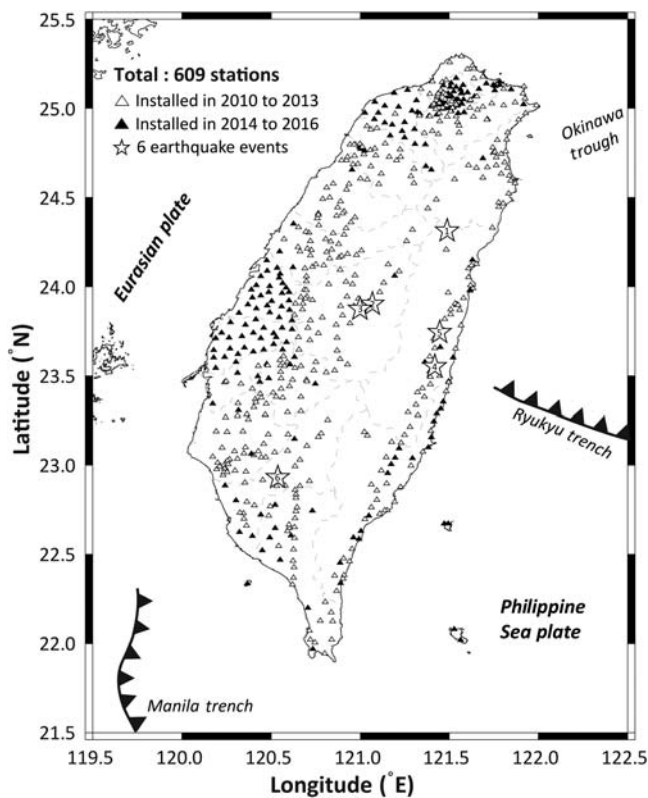


Figure 1. *P*-alert network. There were 609 stations in October 2016. The figure also shows the station density change with time, the epicenter of six events, and important faults around Taiwan.

ters, estimate empirical site effects, predict the intensity and arrival time, and issue warnings to the corresponding area. Although traditional regional EEWSs can provide the location of the earthquake, this advantage can introduce some problems. Earthquake location estimation is bound to have substantial uncertainty, especially for offshore earthquakes, regardless of which location search method is used, the Geiger method (Geiger, 1912) or the Voronoi cell method (Sambridge, 1999). To make things worse, inaccuracies from location estimation will contaminate the rest of the calculations and lead to biased ground-motion predictions or incorrect shaking intensity estimations as a result of applying an improper distance correction (Wu *et al.*, 1998). Additionally, earthquake source directivity effects and radiation patterns are not included in regional EEWS shaking intensity estimations.

The other type of EEWS is the on-site EEWS, which issues warnings directly from on-site ground-motion observations. In Taiwan, one such system is *P*-alert, which is a dense seismic network with 609 low-cost stations in total (Wu and Lin, 2013; Wu *et al.*, 2013, 2016; Wu, 2015). Some of the disadvantages of an on-site EEWS are a relatively large bias in magnitude determination (Wu and Kanamori, 2005), possible station malfunctions, and noise spikes.

Based on the success of the *P*-alert on-site warnings in Taiwan (Wu *et al.*, 2013, 2016), we now want to extend our reach to regional warnings. In this study, we propose a

nontraditional framework of regional EEWSs using the *P*-alert on-site warning system. Our regional EEWS framework ShakingAlarm is developed to address the following three questions:

1. How can this regional EEWS provide better precision in magnitude estimation without an earthquake location process and provide more lead time in the peak ground acceleration (PGA) estimation?

ShakingAlarm bypasses location estimation by employing the relationship between the shake contour area and magnitude described by previous studies (Teng *et al.*, 1997; Lin and Wu, 2010b; Kuo, 2013). In addition to magnitude estimation, the predicted PGA is calculated during the process. The predicted shakemap (PSM) based on the predicted PGA is another useful early warning indicator because it almost always converges faster than the observed shakemap as the past event replays presented in this work reveal. The shake contour area is a natural way to represent all of the predicted PGAs from different stations. Employing the area-to-magnitude relationship, ShakingAlarm transforms the area to a magnitude estimation, which by design does not suffer from single-station anomalies.

2. How can this regional EEWS account for the anisotropic attenuation effect?

The anisotropy of PGA attenuation is addressed in previous studies (Campbell, 1997; Liu, 1999; Lin and Wu, 2010a). ShakingAlarm employs a directional binning and calculates the attenuation decay factor in eight directions from each bin.

3. How can this regional EEWS account for the overall source directivity effect both due to changes of position and due to the Doppler effect?

The directivity effect in source ruptures is known and has been discussed in previous studies (Boatwright, 2007; Kanamori *et al.*, 2016). It is known that larger earthquakes generally have a larger fault plane, and one should consider the source moving along a finite fault rather than as a standing point source. There are two causes for the rupture directivity effect. The first cause is the change of position of hypercenter, and the second is the velocity of the moving source (stations along the incoming rupture direction will observe larger accelerations, whereas stations along the outgoing rupture direction will observe smaller accelerations). ShakingAlarm employs the fitting-source method to account for this effect. This method simply picks the largest PGA over time to represent the overall directivity effect.

A series of real-time replays from past inland earthquake events is used to evaluate the performance of our advanced framework ShakingAlarm. The results show that Shaking Alarm can provide a fast and simple yet robust PSM and magnitude estimation and that the method will meet the

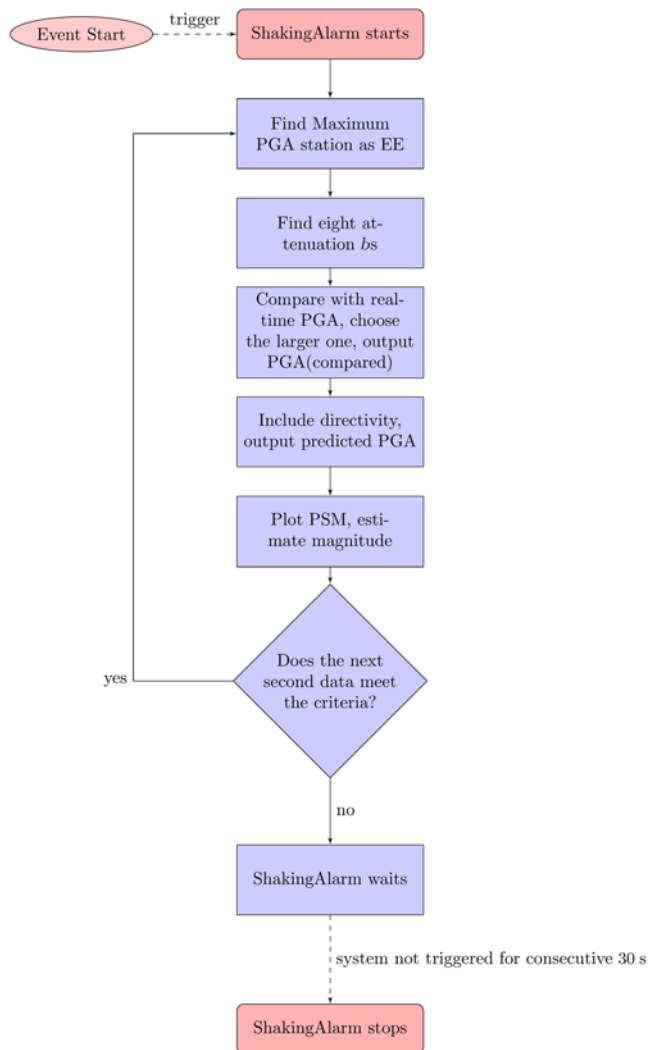


Figure 2. The flowchart of the ShakingAlarm algorithm. The color version of this figure is available only in the electronic edition.

needs of modern risk mitigation, which requires robust and accurate damaged zone determination.

Methodology

Algorithm

When ground-motion data flow into the Earthworm platform, our module PGAComp computes the PGA for every second and then passes the results to the ShakingAlarm module for evaluation. The ShakingAlarm module, the main program used in this project (see Fig. 2), tests the trigger criteria to tell whether it is an event. The trigger criteria (Wu *et al.*, 2013) are empirical and are derived directly from previous on-site *P*-alert studies. If more than six stations are found to meet the criteria (Wu *et al.*, 2013), ShakingAlarm starts a loop of calculations and updates its prediction every second until the trigger criteria fail. When the trigger criteria fail, ShakingAlarm waits for 30 s before the shutdown of the system and the declaration of the event's end.

Find Maximum PGA Station as EE. During the processing loop, ShakingAlarm first picks the maximum PGA as the effective epicenter (EE) and then derives the attenuation relationships between the EE and other stations. The attenuation of seismic waves can be expressed using an expression from a previous study (Wu *et al.*, 2005) as follows:

$$\text{Amp} = \alpha \frac{e^{bR}}{R^n}, \quad (1)$$

in which α is an overall constant, n is the geometrical spreading coefficient, and b can be related to the anelastic attenuation coefficient Q . Empirically, we can simplify equation (1) to

$$\text{PGA}_\tau = \text{PGA}_{\text{EE}} \frac{e^{b_\tau R}}{R^n}, \quad (2)$$

in which b_τ and n are unknowns, PGA_τ is the observed real-time PGA value of a non-EE station τ , PGA_{EE} is the observed real-time PGA value of the EE station, b_τ is the unknown empirical spatial attenuation factor (including site effects between non-EE stations and the EE station) to be derived, and R is the distance from a station to the EE. Figure 3 shows how well this model fits the observed data. This definition of EE can introduce bias caused by offshore events, and is addressed in the Discussion section.

Find Eight Attenuation b_s and n_s . Because seismic waves have an anisotropic attenuation effect, we collect PGA records as inputs from stations in eight directions (N, NE, E, SE, S, SW, W, and NW) between 5 and 20 km from the current EE (set as the origin). Using these records and equation (2), we perform a regression analysis to find best-fitted pairs of b_{eff} and n_{eff} in each of the eight directions.

We choose only stations that are less than 20 km from the EE to calculate b_{eff} and n_{eff} . This choice is based on the fact that the *S* wave will propagate 20 km within 5–6 s (3.5 km/s for a 5- to 6-s window). In other words, including stations that are far from the EE will lead to an incorrect estimation of b_{eff} and n_{eff} because *S* waves may have not arrived at those stations yet. Additionally, all stations that are less than 5 km from the EE are considered equivalent to the EE spatially because their PGAs are similar to the PGA of the EE. These stations are taken out of calculation of b_{eff} and n_{eff} because of possible overweighting for the stations around EE. In other words, if the data for all the stations close to the EE are included, we are likely to underestimate the effect of attenuation, resulting in a smaller lead time. In general, ShakingAlarm can collect data for at least four stations in each direction, although this capability depends heavily on the location of the event. ShakingAlarm will then judge the magnitude of the calculated b_{eff} and n_{eff} to see whether that value is reasonable (less than the preset upperbound, which assumes a modified Mercalli intensity [MMI] IX event). If the values are not reasonable, ShakingAlarm will veto them and use the observed real-time PGA as fallback values.

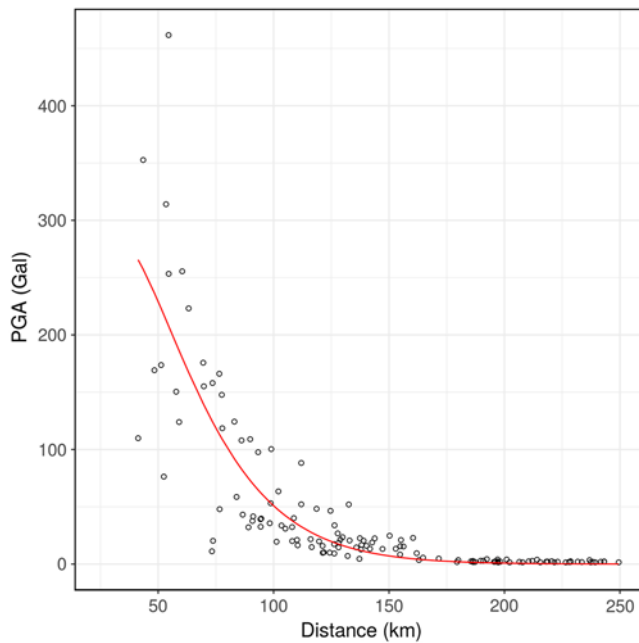


Figure 3. Peak ground acceleration (PGA) versus distance in one direction. The solid line shows how our attenuation model fits the data. The color version of this figure is available only in the electronic edition.

Compare the Predicted PGA with the Observed PGA, Choose the Larger Value as PGA_{compare} . In this step, ShakingAlarm calculates the predicted PGA from the observed PGA by employing the known eight directional b_{eff} s and n_{eff} s. Then, ShakingAlarm compares the predicted PGA and the observed PGA and picks the larger value as compared with PGA, PGA_{compare} . Taking station τ as an illustration, the PGA at a given time is

$$PGA_{\tau,\text{compare}} = \text{Max}[PGA_{\tau,\text{observed}}, PGA_{\tau,\text{predict}}]. \quad (3)$$

Include Source Directivity, Output the Predicted PGA.

ShakingAlarm now accounts for the source directivity effect by the fitting source method, which takes the compared PGA from a different time, $PGA_{\tau,\text{compare}}(t)$, as the input, finds the largest PGA over time, and calls this value the representative PGA, $PGA_{\tau,\text{repr}}$:

$$PGA_{\tau,\text{repr}} = \text{Max}[PGA_{\tau,\text{compare}}(t_1), PGA_{\tau,\text{compare}}(t_2), \dots, PGA_{\tau,\text{compare}}(t_N)], \quad (4)$$

in which the event lasts N seconds. The representative PGA, $PGA_{\tau,\text{repr}}$, is our de facto predicted PGA for station τ . For more details on the fitting source method, see the subsection of the [Source Directivity Effects](#) section.

Plot PSM, Estimate Magnitude. Finally, ShakingAlarm takes the predicted PGA as an input to generate the PSM and then employs the area-to-magnitude equation to estimate the magnitude

$$M_A = 0.002(PGA) \log_{10}(\text{Area}) + 0.279 \log_{10}(\text{Area}) + 4.236, \quad (5)$$

in which M_A is the magnitude derived from the shake contour area. PGA is a given PGA value in Gal; here, we use $PGA = 100$ Gal. Area is the shake contour area in km^2 with acceleration above the given PGA. For more details on the magnitude estimation based on shaking contour area, please see the subsection on magnitude estimation.

Source Directivity Effects

For every second during the earthquake event, we can define the station with largest PGA as the EE. However, it is known that the EE is time dependent during larger events ($M_L > 5.5$) (Cauzzi *et al.*, 2015). To keep track of the overall directivity effect, we propose the fitting-source method, which finds the all-time largest PGA of one station. Taking station τ as an example, after including the time-dependent attenuation, the PGA at t_1 is $PGA_{\tau,\text{compare}}(t_1)$, which depends on both time (t_1) and space (τ). ShakingAlarm will record $PGA_{\tau,\text{compare}}$ at different times and find the largest PGA as the representative PGA. The mathematical expression of representative PGA, $PGA_{\tau,\text{repr}}$, is shown in equation (4). In other words, after the fitting-source method is applied, the representative PGA has only spatial dependency τ , and the representative PGA can be shown by the PSM.

Magnitude Estimation Based on Shaking Contour Area

In a series of studies (Teng *et al.*, 1997; Lin and Wu, 2010b; Kuo, 2013), a regression relationship between shaking contour and magnitude was established. The latest of them (Kuo, 2013) used 42 intermediate to large earthquakes (from M_w 5.0 to 7.6) between 1995 and 2012 as inputs. To derive the shaking contour map, the authors partitioned Taiwan into a grid of $0.05^\circ \times 0.05^\circ$ cells. For each grid cell, there is a centroid. The PGA for every centroid of the grid cell can be interpolated from station PGAs:

$$PGA_{\text{Grid}} = \frac{\sum_{\tau=1}^n \frac{PGA_{\tau,\text{repr}}}{D_\tau^2}}{\sum_{\tau=1}^n \frac{1}{D_\tau^2}} D_\tau < 60 \text{ km}, \quad (6)$$

in which $PGA_{\tau,\text{repr}}$ is the representative PGA for station τ and D_τ is the distance between that station and the grid point. Once all the grid cell's PGA values are found, the PGA shaking contour areas can be calculated; for example, by using the shaking contour area for $PGA > 100$ Gal. The regression relation is equation (5), and the standard deviation for choosing $PGA = 100$ Gal is 0.39. The equation is similar in format to that in Lin and Wu (2010b) but with more parameters to be determined.

Table 1
Six Recent Events Used in This Study and Their Parameters

Event	Origin Time (UTC) (yyyy/mm/dd hh:mm:ss)	Hypocenter			CWB M_L	M_w
		Longitude (°E)	Latitude (°N)	Depth (km)		
A	2013/03/07 03:36:46	121.49	24.31	15.2	5.6	5.5
B	2013/03/27 02:03:20	121.07	23.90	15.4	6.1	6.1
C	2013/06/02 05:43:04	121.00	23.87	10.0	6.3	6.2
D	2013/10/31 12:02:09	121.42	23.55	19.5	6.3	6.3
E	2014/05/21 00:21:14	121.45	23.74	18.0	5.9	5.9
F	2016/02/05 19:57:27	120.54	22.93	16.7	6.4	6.4

CWB, Central Weather Bureau.

Data and Results

The *P*-alert seismic network is a dense array of 609 stations in Taiwan. The earthquake sensors of a *P*-alert station are low-cost microelectromechanical systems acceleration sensors (Holland, 2003) that return a series of real-time acceleration data in three directions in 16-bit blocks at a 100-Hz sampling rate and a maximum recording range of $\pm 2g$. The central computer at National Taiwan University receives the ground-motion data from the *P*-alert network in real time and stores all the data in the Earthworm platform (Johnson *et al.*, 1995). The collected data stored in Earthworm are ready for further processing.

For this project, we choose six recent inland earthquake events with local magnitudes larger than 5.5 between 2013 and 2016 to test the effectiveness of ShakingAlarm (see Table 1 for details).

These past events were measured by the *P*-alert network, and the waveforms of stations are stored within the Earthworm platform. Tankplayer, a playback module of Earthworm, is used to replay the past waveforms. Tankplayer will replay the waveform by sending out 1-s packages of each station for ShakingAlarm to analyze. Because these packages are replays of events, the event origin time is already known, and zero on the time axis always refers to the event origin in this study.

Figure 4 shows the regression between 14 s and the final PGA of events A–E. This figure shows an overall increasing trend in the coefficient of determination (r^2). Based on the given results, we choose to focus on the latest two events E and F. Although E is not the event with the second largest r^2 , we still choose it as an example. We choose to discuss two event simulations in more detail. Event F is chosen because it shows the most recent network configuration and the results have the highest r^2 . In addition, event E is chosen because its estimation (1) is based on the second largest station density, (2) is considered successful because its r^2 is sufficiently large, and (3) showcases an event in eastern Taiwan.

Figures 5 and 6 are plots comparing the PSM and the observed shakemap of events E and F. At the 6th and 10th seconds, the PSMs exhibit smooth circular contours, while their observed counterparts show very noncircular contour shapes, for example, an 80-Gal contour in part (b) of

Figures 5 and 6. At the 14th second, both PSMs are close in shape to the final reported shakemap.

Figure 7 shows the comparison of event F between ShakingAlarm and CWB's regional EEWS with respect to the final reported shakemap. In the log–log scale, the linear regression r^2 of CWB is 0.603, whereas the r^2 of ShakingAlarm is 0.899. The standard deviation σ of CWB is 0.2, whereas the σ of ShakingAlarm is 0.13.

Figure 8 shows a comparison between the predicted PGA and the observed real-time PGA for event E (Table 1). We choose to show three stations at three different distances as a representation of all stations. Near station W008 (right middle, 27 km away from the epicenter), the predicted PGA uniformly dominates the real-time PGA from the beginning (6th second) until the real-time PGA reaches a common stable value (142.80 Gal) near the 11th second. At station W012 (right top, 52 km away from the epicenter), the predicted PGA uniformly dominates the real-time PGA until both the real-time PGA and the predicted PGA reach a common stable value (63.62 Gal) at the 17th second. At the more distant station W12A (right bottom, 72 km away from the epicenter), the predicted PGA reaches a stable value (33.86 Gal) at the 8th second, and the predicted PGA dominates until the real-time PGA reaches a stable value of 27.31 Gal at the 22nd second. There is a 24% difference between the predicted PGA and the observed real-time PGA, which can occur when one station at a time has a large predicted PGA.

The gray solid line indicates the time ShakingAlarm will predict an MMI V shaking level, which corresponds to 30 Gal, and the gray dotted line indicates the time that Strategies and Tools for Real Time Earthquake Risk Reduction (REAKT; Parolai *et al.*, 2015), another algorithm we tested for comparison, will predict an MMI V shaking level. At station W012, ShakingAlarm issues a warning at the 11th second, whereas REAKT issues a warning at the 12th second. At station W008, ShakingAlarm issues warning at the 9th second, whereas REAKT issues a warning at the 8th second. At station W12A, ShakingAlarm does not issue a warning at all, whereas REAKT issues a warning at the 16th second. The final observed PGA does not reach MMI V, and therefore, REAKT gives a false alarm.

Figure 9 shows the comparison between the predicted PGA and the observed real-time PGA for event F (Table 1). Near station W21B (left middle, 27 km away from the epicenter), the predicted PGA is similar to the real-time PGA from the 6th to 11th second. At the 12th second, the dominance of the predicted PGA (311.14 Gal) begins and lasts until a common stable value (452.57 Gal) is reached at approximately the 16th second. At station L004 (left bottom, 35 km away from epicenter), the predicted PGA at the 12th second reaches a stable value at 261.90 Gal, which is a

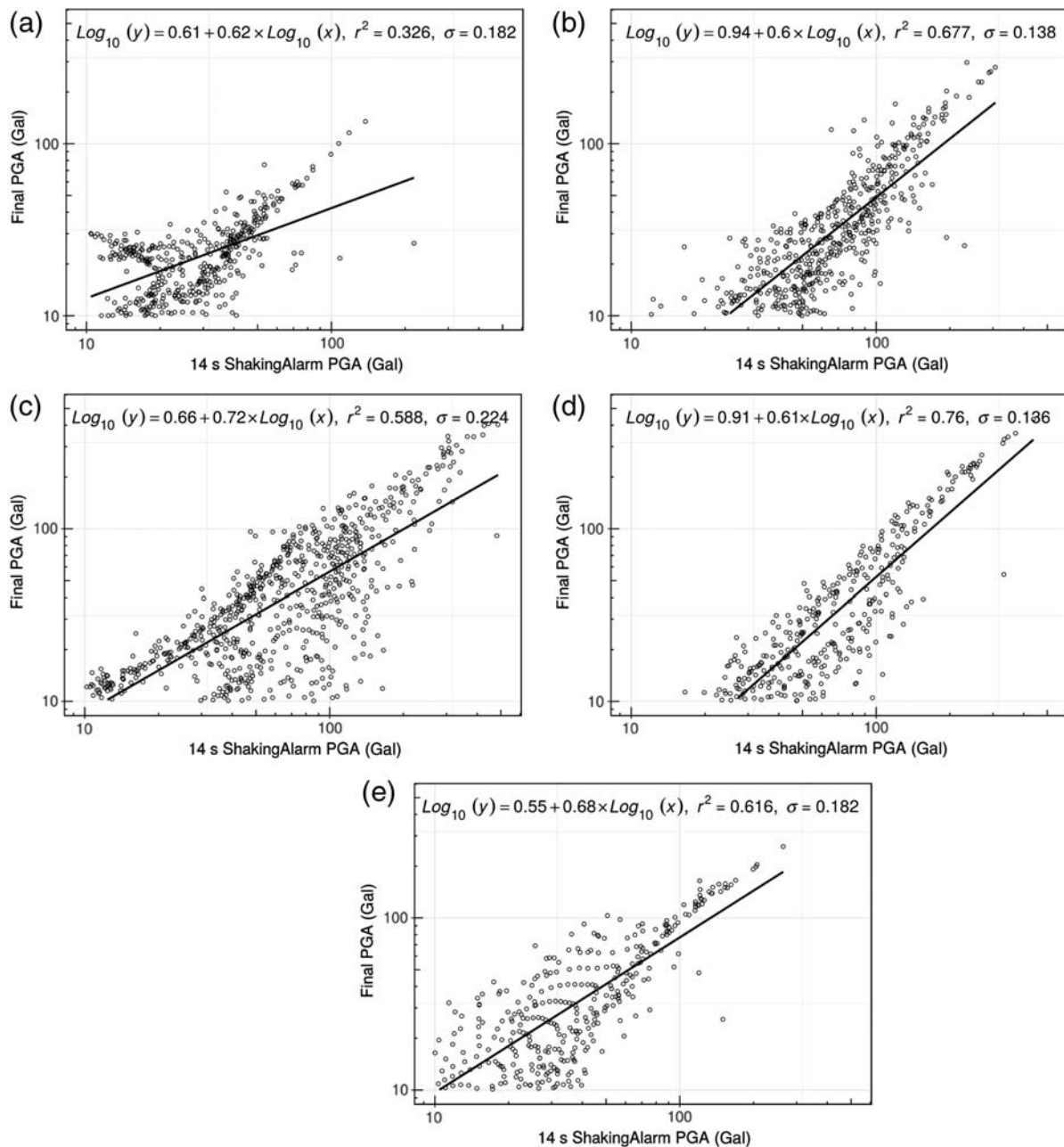


Figure 4. The regressions of 14 s and final PGA. The results of the first five events: (a) event A, (b) event B, (c) event C, (d) event D, and (e) event E.

difference of $\sim 10\%$ compared with the final real-time PGA value of 237.30 Gal. At the more distant station W196 (left top, 63 km away from the epicenter), the predicted PGA dominates the PGA uniformly from the beginning until both measures reach a common stable value (195.05 Gal) at approximately the 23rd second.

The gray solid line indicates the time that ShakingAlarm will predict an MMI V shaking level, and the gray dotted line indicates the time that REAKT will predict an MMI V shaking level. At station W196, ShakingAlarm issues a warning at the 8th second, whereas REAKT issues a warning at the

22nd second. At station W21B, ShakingAlarm issues a warning at the 10th second, whereas REAKT issues a warning at the 10th second as well. At station L004, ShakingAlarm issues a warning at the 11th second, whereas REAKT issues a warning at the 11th second as well.

We choose to present the near site as 27 km from the epicenter because the blind zone is at ~ 30 km. Deep inside the blind zone, the predicted PGA is very similar to the observed PGA.

The predicted magnitude difference ($M - M_w$) versus time is shown in Figure 10. All the events converge on a

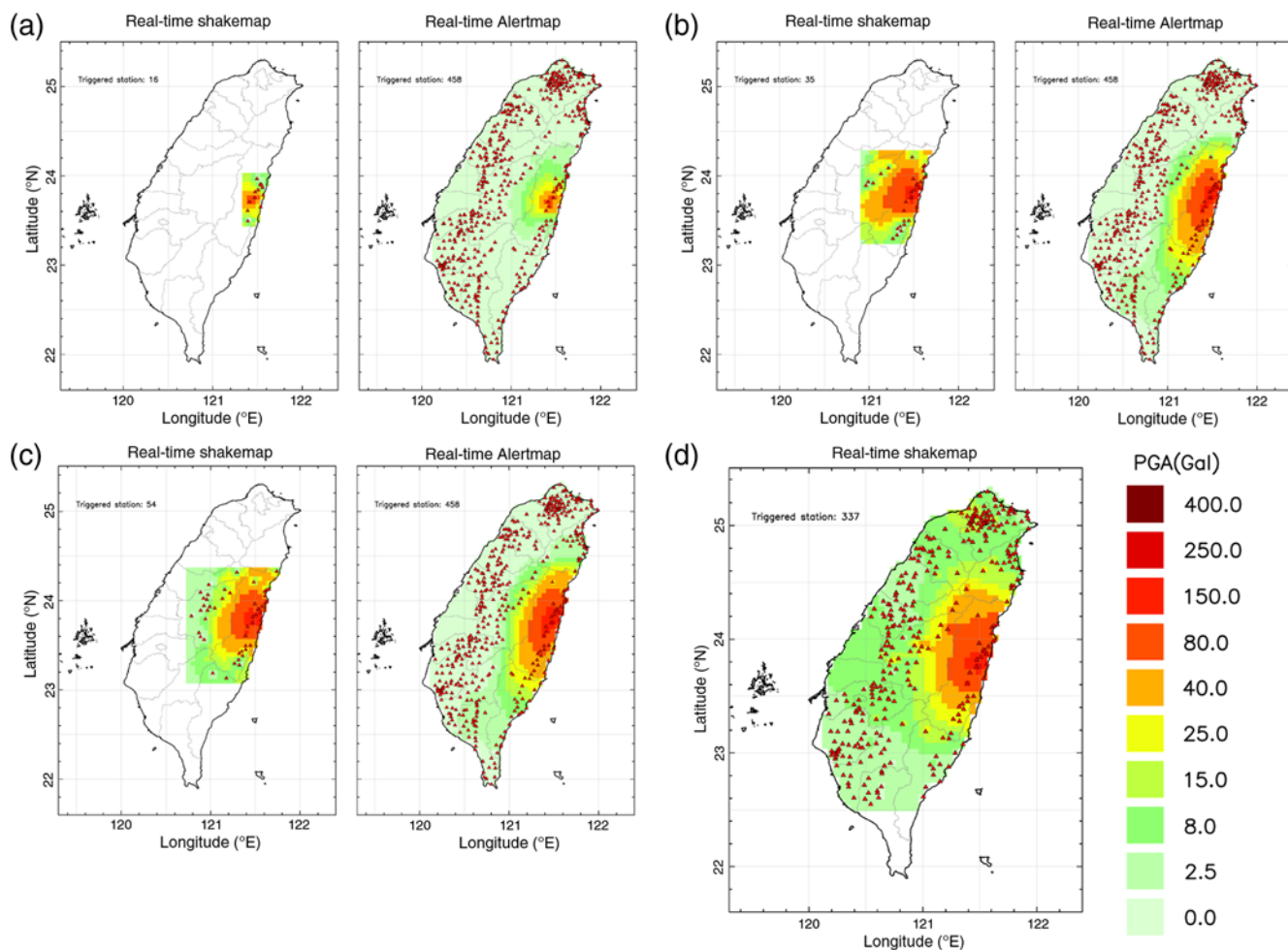


Figure 5. Replay results of event E in Table 1. A series of comparison graphs of the predicted shakemap (PSM) and the observed shakemap. (a) Observed versus predicted, at 6th second; (b) observed versus predicted, at 10th second; (c) observed versus predicted, at 14th second; and (d) final reported shakemap. The color version of this figure is available only in the electronic edition.

0.5-magnitude deviation in 10 s, and they arrive at stable values in ~ 18 s except for event (D). A closer look at the comparison between our predicted magnitude and observed magnitude (Table 2) shows that at the 6th second (first), the predicted magnitude is closer to M_w than the observed magnitude. At the 10th second (stable), the two magnitudes all converge to M_w .

Discussion

PSM Performance

In this article we developed ShakingAlarm, an add-on regional warning system based on the existing P -alert on-site seismic network. Exploiting P -alert's dense network, ShakingAlarm can estimate attenuation factors in eight directions and predict the shaking contour in PSM and magnitude. As a result, in the 14th second in the PSM (Figs. 5 and 6), ShakingAlarm converges better than the existing regional warning system by CWB in Taiwan (Fig. 7).

PSM Source Directivity

Although many studies have focused on the connection between the observed shakemap (or final reported shakemap) and rupture (Bose *et al.*, 2015; Hoshiya and Aoki, 2015), making this connection is still quite a challenging task. For one, the Doppler effect due to the directivity velocity is often neglected for the sake of simplicity. Additionally, the shake contour is difficult to identify because of the presence of speckle ground motion, as the numerical wave simulation shows (Hoshiya and Aoki, 2015). ShakingAlarm handles both of these challenges to some extent. The fitting-source method used in ShakingAlarm accounts for both the source position change effect and Doppler effect. Additionally, the shake contours predicted by ShakingAlarm are smoother and more elliptical than the observed shake contour (see the 80-Gal contour in Figs. 5 and 6). It is possible that ShakingAlarm's PSM embeds the information of the source directivity. The directional change along the stretching axis of the predicted shake contour might infer the rupture

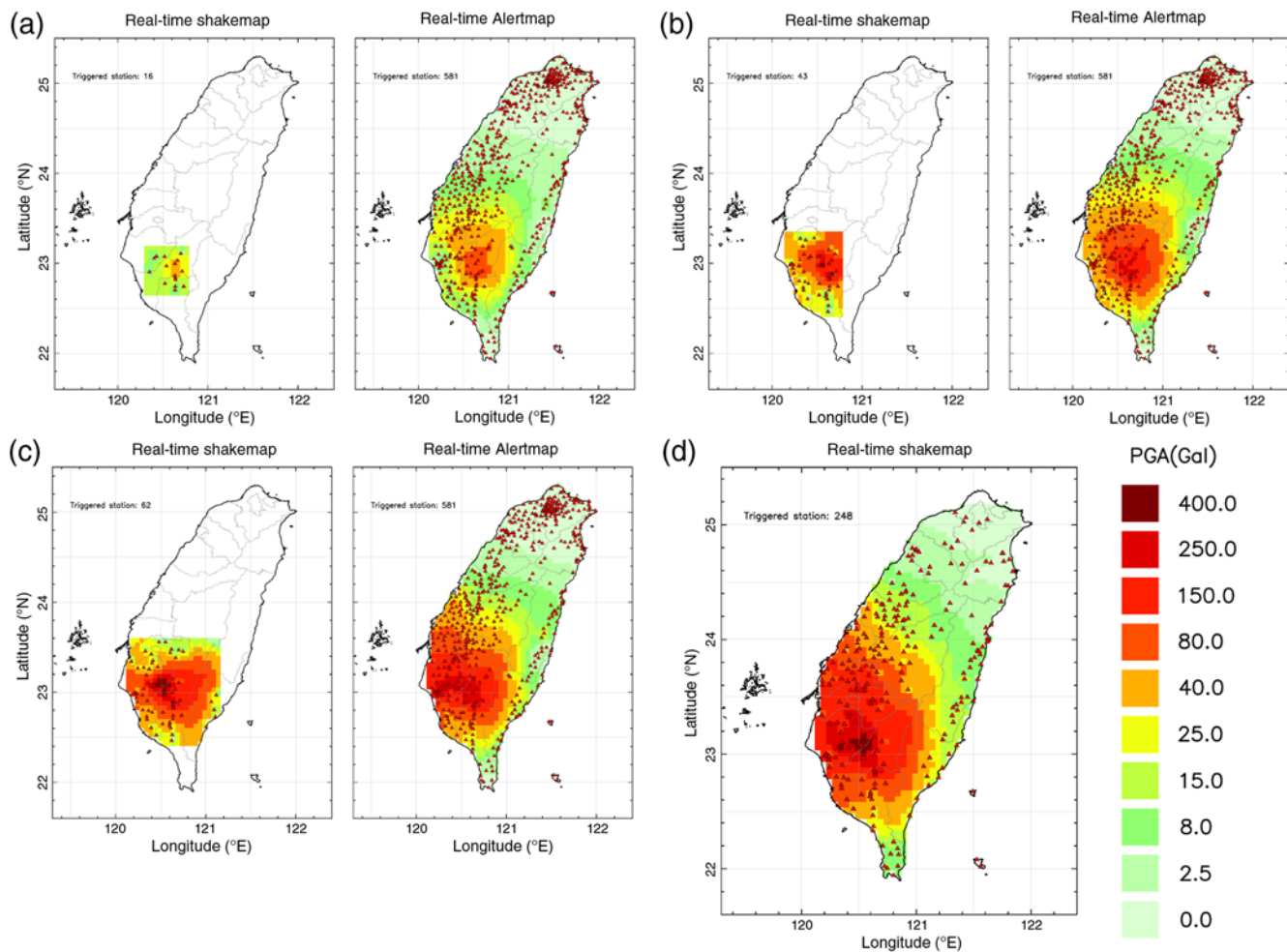


Figure 6. Replay results of event F in Table 1. A series of comparison graphs of the PSM and the observed shakemap. (a) Observed versus predicted, at 6th second; (b) observed versus predicted, at 10th second; (c) observed versus predicted, at 14th second; and (d) final reported shakemap. The color version of this figure is available only in the electronic edition.

direction with velocity, but this inference is empirical, and further investigations are needed.

Predicted PGA Performance

Second, as a consistency check, we compare the predicted PGA with another on-site early warning method (REAKT). The results (Figs. 8 and 9) show good consistency in most cases, but some improvements are shown in the other cases. When ShakingAlarm is integrated into *P*-alert in the future, the new on-site warning system will receive different information from different sources (ShakingAlarm provides the predicted PGA, and *P*-alert provides Pd and τ_c) and will have a different performance than ShakingAlarm. The overall performance of the integrated new system is beyond the scope of this article and will be explored in our future work.

Magnitude Estimation Performance

Third, the performance of magnitude estimation is tested against past events. The results (Fig. 10) show that the area-based magnitude can consistently reach a ± 0.5 deviation

from the final estimation within 20 s. A closer look at the last two events (E and F in Table 2) shows that the first report of the M_A of the predicted PSM is better than the M_A of the observed real-time PSM. The final convergence value of the M_A of the predicted PSM is similar in magnitude to the M_A of the observed PSM.

Although the EE can only be onshore with this approach, the area-based magnitude estimation can still be a useful reference because the logarithm of the area does not deviate much for different percentages of the shake contour area. For a numerical demonstration, we assume that there is an offshore earthquake with only 50% of the shake contour area (PGA = 100 Gal) being inland. Comparing with the case in which 100% of the shake contour area is inland, the magnitude central value difference is

$$\begin{aligned} \Delta M_A &= M_A(A) - M_A(0.5A) \\ &= 0.002 \times 100 \times \log_{10}(2) + 0.279 \times \log_{10}(2) \approx 0.14, \end{aligned} \quad (7)$$

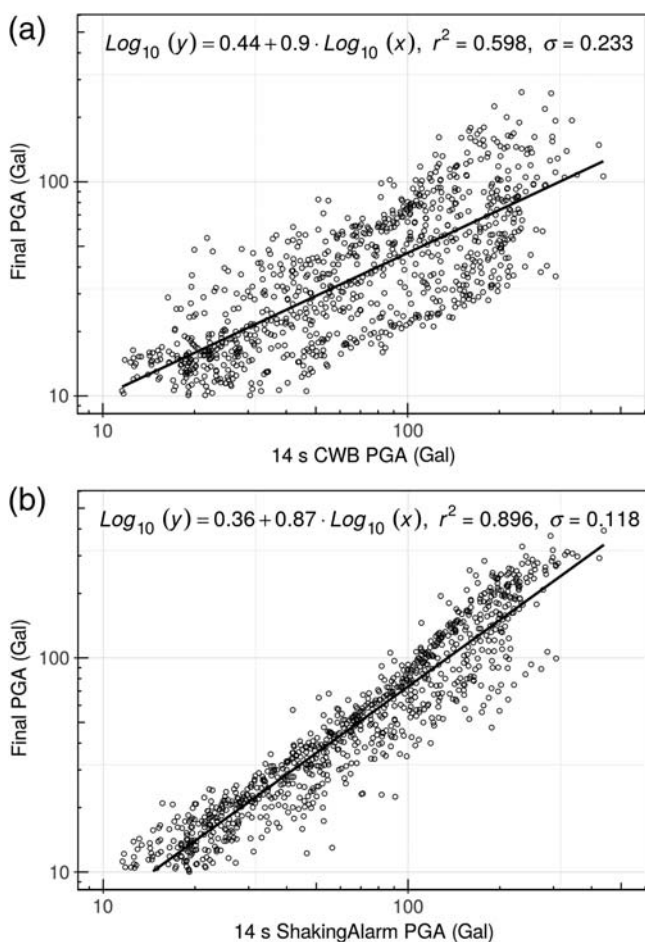


Figure 7. The comparison of event F between 14 s Central Weather Bureau (CWB) PSM results and 14 s ShakingAlarm PSM results. (a) Final reported shakemap versus CWB 14 s shakemap. (b) Final reported shakemap versus ShakingAlarm 14 s shakemap.

which employs equation (5) and shows that the magnitude deviates by only 0.14 for absence of one half of the area; in other words, the area-based magnitude determination is quite robust. Even for the extreme case in which 25% of the area is inland, the magnitude central value difference is ~ 0.29 .

Limitations

There are a few limitations of this study. ShakingAlarm is primarily focused on inland, shallow, and large earthquakes, which cause great damage. For offshore earthquakes, the EE is far from the real epicenter. The corresponding b and n values might also deviate from the proper values (the values if the earthquake is inland), which might eventually result in less lead time in the PGA estimation.

Another limitation is the density of stations around the epicenter, which might explain the performance difference between the first four events (A–D) and the last two events (E and F). The density of stations was lower at that time, which will inevitably affect the validity of the algorithm. There were only 401 stations in the P -alert network in 2013. Later, this number increased to 506 stations in 2014 and

finally reached 609 stations in 2016. One way to see this constant increasing density resulting in performance improvements over the years is to examine the trend of increasing regression r^2 in Figures 4 and 7.

Based on the performance difference in the predicted PGA and magnitude prediction for early events, this study suggests that station density around the epicenter may play a crucial role in our PGA estimation algorithm. The spatial attenuation pair b and n will be unreliable when the epicenter is located in a sparse or inhomogeneous array of stations. The bias of b and n will propagate throughout the following steps of the shakemap and magnitude estimations. This study recommends an increase in the density of the P -alert network for better performance. Additionally, the quality of Internet-transmitted data can affect performance. Information packages that are either incomplete or delayed will be abandoned in favor of cleaner data. ShakingAlarm will automatically find the last five seconds of clean data to proceed, which is embedded in our trigger criteria in the ShakingAlarm module. The quality of the waveform data was significantly inferior before 2015. A series of improvements were undertaken in 2015, including (1) upgrading the client-side loading capacity to enable larger data transmission and (2) fixing broken stations and ensuring on-site Internet reliability. An improvement in data transmission may be one of the reasons explaining the performance enhancement observed in the last two events.

Related Work

Regarding EEWs, REAKT (Parolai *et al.*, 2015) skillfully combines both PGA and peak ground velocity to produce a more accurate on-site warning indicator. Regarding the fault source directivity, the Finite-fault rupture Detector (FinDer) algorithm (Bose *et al.*, 2015) employs the ground-motion pattern to infer the fault position change with time. The work by Hoshiya and Aoki (2015) focuses on the numerical simulation of source rupture and seismic waves. Huang *et al.* (2017) develop a mathematical framework to describe the effect of rupture velocity on ground motion. ShakingAlarm keeps track of both effects at the same time.

Conclusions

ShakingAlarm can provide three types of warnings: predicted PGA, PSM, and magnitude estimation. First, ShakingAlarm provides the predicted PGA of a specific station by employing the time-dependent anisotropic peak ground-motion attenuation relationship. The results obtained by replaying past events (E and F) show that in ShakingAlarm, the predicted PGA outside the blind zone (30 km from epicenter) reaches the CWB intensity faster than the traditional regional method, which is the observed real-time PGA. The quantitative results are represented by the warning time of MMI V of the predicted PGA. The replay results show the possibility of reliable predicted PGA at 10 s from origin time. Second, ShakingAlarm

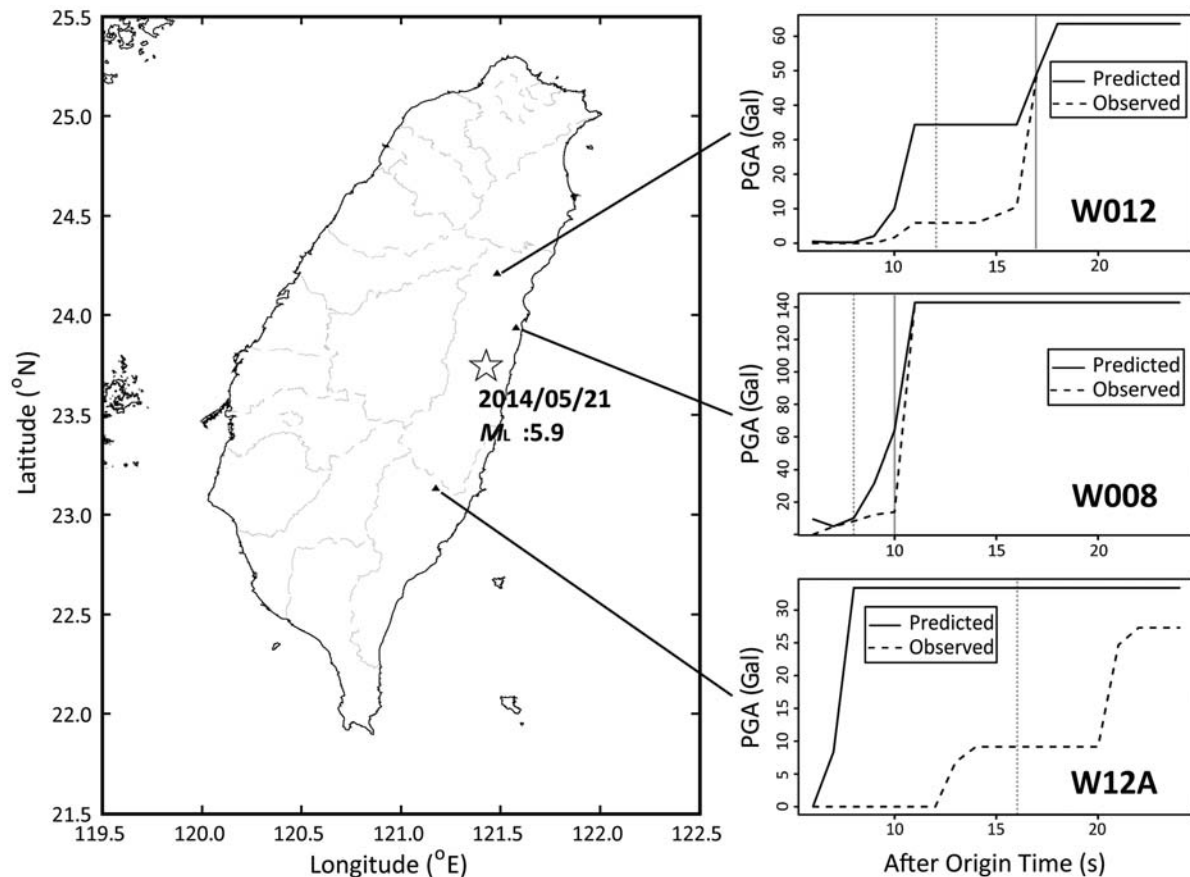


Figure 8. PGA replay of event E in Table 1. The PGAs of three stations are plotted as both the predicted PGA and the observed PGA. (Right) From top to bottom, station W012 is 52 km away from the epicenter, station W008 is 27 km away from the epicenter, and station W12A is 72 km away from the epicenter. The gray solid line indicates the time ShakingAlarm will predict a modified Mercalli intensity (MMI) V shaking level, and the gray dotted line indicates the time REAKT (Strategies and Tools for Real Time Earthquake Risk Reduction) will predict an MMI V shaking level.

provides the PSM of the event. The provided PSMs have already included directivity and radiation pattern effects, which is a significant improvement in shaking prediction (comparing the 14th-second PSM with the 14th-second CWB regional PSM). The convergence of PSMs to the final PSM occurs within 14 s in the replay. Third, ShakingAlarm provides a shake contour area-based magnitude estimation. This magnitude estimation is robust and does not require traditional earthquake location estimation. As a result, the estimation can avoid a potential bias in magnitude determination due to mislocation.

The convergence of magnitude estimation to M_w occurs within 20 s in the replay. When integrated with the existing on-site warning P -alert network, ShakingAlarm, our advanced regional warning system, is expected to set an even higher standard for future disaster reduction and hazard mitigation.

Data and Resources

Waveform data from the P -alert seismic network were obtained from the seismological lab in National Taiwan

Table 2
Magnitude Comparison of Predicted, Real-Time, CWB, and U.S. Geological Survey (USGS)

Origin Time (UTC) (yyyy/mm/dd) (hh:mm:ss)	Report	This Study (Predicted PGA)		Observed PGA			
		Magnitude (M_A)	Reporting Time (s)	Magnitude (M_A)	Reporting Time (s)	CWB (M_L)	USGS (M_w)
2014/05/21 (E)	First	5.3	6	5.0	6	5.9	5.6
00:21:14	Stable	5.9	11	5.8	10		
2016/02/05 (F)	First	5.5	6	5.0	7	6.4	6.4
19:57:27	Stable	6.3	17	6.3	25		

Only the last two events (events E and F) are presented in Table 1. PGA, peak ground acceleration.

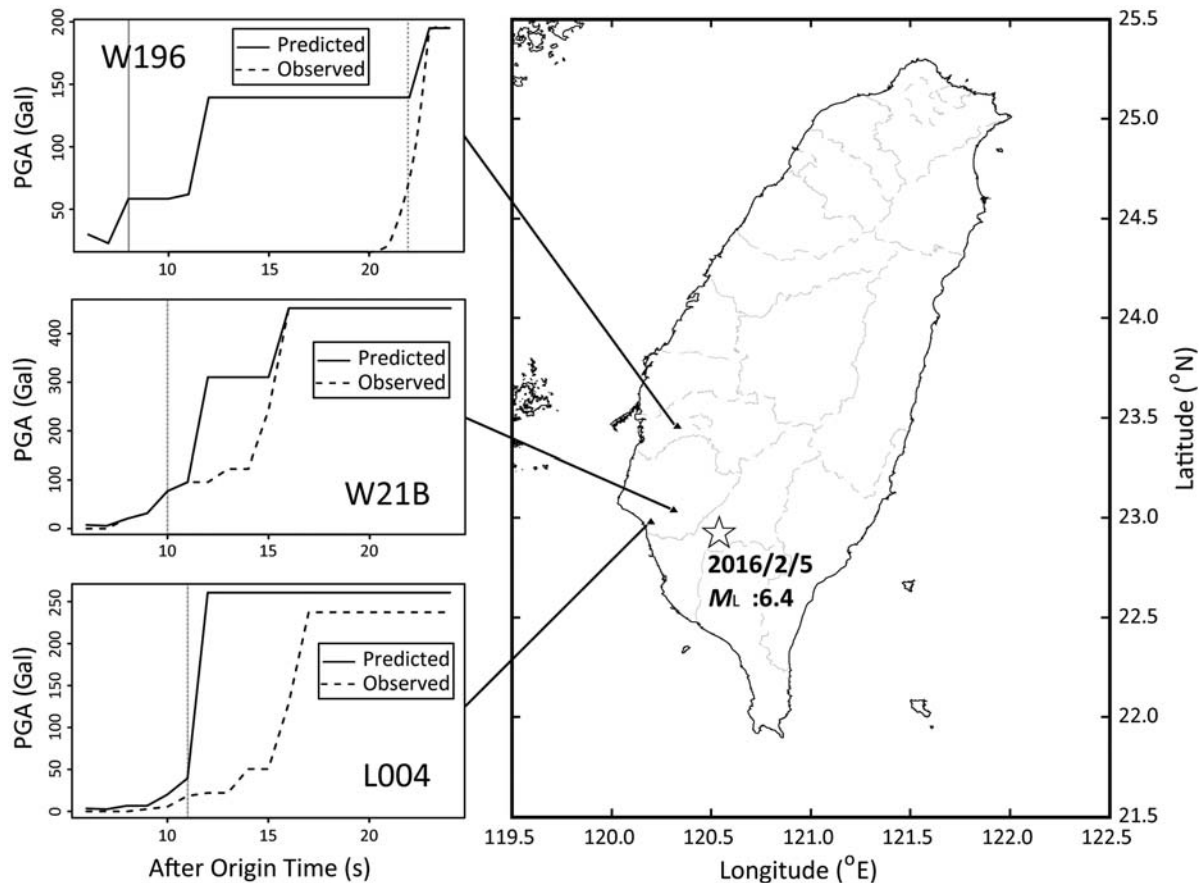


Figure 9. PGA replay of event F in Table 1. The PGAs of three stations are plotted as both the predicted and the observed PGA. (Left) From top to bottom, station W196 is 63 km away from the epicenter, station W21B is 27 km away from the epicenter, and station L004 is 35 km away from the epicenter. The gray solid line indicates the time ShakingAlarm will predict an MMI V shaking level, and the gray dotted line indicates the time REAKT will predict an MMI V shaking level.

University (<http://seismology.gi.ntu.edu.tw>, last accessed February 2018). The regional earthquake early warning (EEW) data were obtained from the Central Weather Bureau in Taiwan (<http://www.cwb.gov.tw>, last accessed February 2018).

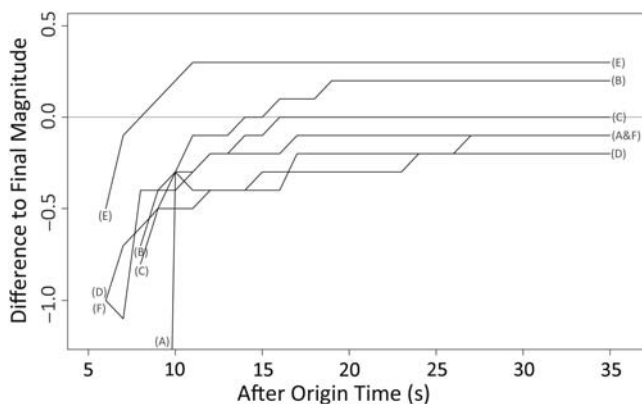


Figure 10. Replay results of the magnitude difference (predicted magnitude minus M_w) versus time (start from origin time). Note that (A)–(F) indicate the earthquake events recorded in Table 1.

Acknowledgments

The authors would like to thank Da-Yi Chen for providing the Central Weather Bureau (CWB) data. The authors also want to thank the anonymous reviewers for their valuable comments that helped improve this article. This work was supported by the Ministry of Science and Technology (MOST) of Taiwan. B. M. Y. and Y.-M. W. were supported under MOST 105-2116-M-002-002. T.-C. H. was supported under MOST 105-2811-M-001-036.

References

- Allen, R. M., H. Brown, M. Hellweg, O. Khainovski, P. Lombard, and D. Neuhauser (2009). Real-time earthquake detection and hazard assessment by ElarmS across California, *Geophys. Res. Lett.* **36**, L00B08, doi: [10.1029/2008GL036766](https://doi.org/10.1029/2008GL036766).
- Allen, R. M., P. Gasparini, O. Kamigaichi, and M. Bose (2009). The status of earthquake early warning around the world: An introductory overview, *Seismol. Res. Lett.* **80**, no. 5, 682–693, doi: [10.1785/gssrl.80.5.682](https://doi.org/10.1785/gssrl.80.5.682).
- Boatwright, J. (2007). The persistence of directivity in small earthquakes, *Bull. Seismol. Soc. Am.* **97**, 1850–1861, doi: [10.1785/0120050228](https://doi.org/10.1785/0120050228).
- Bose, M., C. Felizardo, and T. H. Heaton (2015). Finite-fault rupture Detector (FinDer): Going real-time in Californian ShakeAlert warning system, *Seismol. Res. Lett.* **86**, no. 6, 1692–1704, doi: [10.1785/0220150154](https://doi.org/10.1785/0220150154).
- Campbell, K. W. (1997). Empirical near-source attenuation relationships for horizontal and vertical components of peak ground acceleration, peak ground velocity, and pseudo-absolute acceleration response spectra, *Seismol. Res. Lett.* **68**, no. 1, 154–179, doi: [10.1785/gssrl.68.1.154](https://doi.org/10.1785/gssrl.68.1.154).

- Cauzzi, C., E. Faccioli, M. Vanini, and A. Bianchini (2015). Updated predictive equations for broadband (0.01–10 s) horizontal response spectra and peak ground motions, based on a global dataset of digital acceleration records, *Bull. Earthq. Eng.* **13**, 1587–1612, doi: [10.1007/s10518-014-9685-y](https://doi.org/10.1007/s10518-014-9685-y).
- Clinton, J., A. Zollo, A. Marmureanu, C. Zulfikar, and S. Parolai (2016). State-of-the-art and future of earthquake early warning in the European region, *Bull. Earthq. Eng.* **14**, 2441–2458, doi: [10.1007/s10518-016-9922-7](https://doi.org/10.1007/s10518-016-9922-7).
- Cooper, J. D. (1868). Earthquake indicator, *San Francisco Bulletin*, 3 November 1868.
- Espinosa-Aranda, J. E., A. Jimeénez, G. Ibarrola, F. Alcantar, A. Aguilar, M. Inostroza, and S. Maldonado (1995). Mexico City seismic alert system, *Seismol. Res. Lett.* **66**, no. 6, 42–53, doi: [10.1785/gssrl.66.6.42](https://doi.org/10.1785/gssrl.66.6.42).
- Geiger, L. (1912). Probability method for the determination of earthquake epicenters from the arrival time only (translated from Geiger's 1910 German article), *Bull. St. Louis Univ.* **8**, no. 1, 56–71.
- Holland, A. (2003). Earthquake data recorded by the MEMS accelerometer: Field testing in Idaho, *Seismol. Res. Lett.* **74**, no. 1, 20–26, doi: [10.1785/gssrl.74.1.20](https://doi.org/10.1785/gssrl.74.1.20).
- Hoshiba, M., and S. Aoki (2015). Numerical shake prediction for earthquake early warning: Data assimilation, real-time shake mapping, and simulation of wave propagation, *Bull. Seismol. Soc. Am.* **105**, 1324–1338, doi: [10.1785/0120140280](https://doi.org/10.1785/0120140280).
- Hsiao, N. C., Y. M. Wu, T. C. Shin, L. Zhao, and T. L. Teng (2009). Development of earthquake early warning system in Taiwan, *Geophys. Res. Lett.* **36**, L00B02, doi: [10.1029/2008GL036596](https://doi.org/10.1029/2008GL036596).
- Hsiao, N. C., Y. M. Wu, L. Zhao, D. Y. Chen, W. T. Huang, K. H. Kuo, and P. L. Leu (2011). A new prototype system for earthquake early warning in Taiwan, *Soil Dynam. Earthq. Eng.* **31**, no. 2, 201–208, doi: [10.1016/j.soildyn.2010.01.008](https://doi.org/10.1016/j.soildyn.2010.01.008).
- Huang, H. H., N. Aso, and V. C. Tsai (2017). Toward automated directivity estimates in earthquake moment tensor inversion, *Geophys. J. Int.* **211**, 1062–1076, doi: [10.1093/gji/ggx354](https://doi.org/10.1093/gji/ggx354).
- Johnson, C. E., A. Bittenbinder, B. Bogaert, L. Dietz, and W. Kohler (1995). Earthworm: A flexible approach to seismic network processing, *IRIS Newsletter* **14**, no. 2, 1–4.
- Kanamori, H., E. Hauksson, and T. Heaton (1997). Real-time seismology and earthquake hazard mitigation, *Nature* **390**, 461–464, doi: [10.1038/37280](https://doi.org/10.1038/37280).
- Kanamori, H., L. Ye, B.-S. Huang, H.-H. Huang, S.-J. Lee, W.-T. Liang, Y.-Y. Lin, K.-F. Ma, Y.-M. Wu, and T.-Y. Yeh (2016). A strong-motion hot spot of the 2016 Meinong, Taiwan, earthquake ($M_w = 6.4$), *Terr. Atmos. Ocean. Sci.* doi: [10.3319/TAO.2016.10.07.01](https://doi.org/10.3319/TAO.2016.10.07.01).
- Kuo, K.-H. (2013). Development of a real-time shaking map system using low cost acceleration sensors and its application for earthquake early warning, *Master's Thesis*, Department of Geosciences, National Taiwan University.
- Lin, T. L., and Y. M. Wu (2010a). Magnitude determination using strong ground-motion attenuation in earthquake early warning, *Geophys. Res. Lett.* **37**, L07304, doi: [10.1029/2010GL042502](https://doi.org/10.1029/2010GL042502).
- Lin, T. L., and Y. M. Wu (2010b). Magnitude estimation using the covered areas of strong ground motion in earthquake early warning, *Geophys. Res. Lett.* **37**, L09301, doi: [10.1029/2010GL042797](https://doi.org/10.1029/2010GL042797).
- Liu, K. S. (1999). Attenuation relationships for strong ground motion in Taiwan, *Ph.D. Thesis*, Institute of Geophysics, National Central University, Taiwan.
- Nakamura, Y. (1988). On the urgent earthquake detection and alarm system (UrEDAS), *Proc. of the 9th World Conf. on Earthquake Engineering*, Vol. 7, 673–678.
- Parolai, S., D. Bindi, T. Boxberger, C. Milkereit, K. Fleming, and M. Pittore (2015). On-site early warning and rapid damage forecasting using single stations: Outcomes from the REAKT project, *Seismol. Res. Lett.* **86**, no. 5, 1393–1404, doi: [10.1785/0220140205](https://doi.org/10.1785/0220140205).
- Sambridge, M. (1999). Geophysical inversion with a neighborhood algorithm—I. Searching a parameter space, *Geophys. J. Int.* **138**, 479–494, doi: [10.1046/j.1365-246X.1999.00876.x](https://doi.org/10.1046/j.1365-246X.1999.00876.x).
- Satriano, C., Y. M. Wu, A. Zollo, and H. Kanamori (2011). Earthquake early warning: Concepts, methods and physical grounds, *Soil Dynam. Earthq. Eng.* **31**, no. 2, 106–118, doi: [10.1016/j.soildyn.2010.07.007](https://doi.org/10.1016/j.soildyn.2010.07.007).
- Teng, T. L., L. Wu, T. C. Shin, Y. B. Tsai, and W. H. Lee (1997). One minute after: Strong-motion map, effective epicenter, and effective magnitude, *Bull. Seismol. Soc. Am.* **87**, 1209–1219.
- Wu, Y. M. (2015). Progress on development of an earthquake early warning system using low-cost sensors, *Pure Appl. Geophys.* **172**, no. 9, 2343–2351, doi: [10.1007/s00024-014-0933-5](https://doi.org/10.1007/s00024-014-0933-5).
- Wu, Y. M., and H. Kanamori (2005). Experiment on an onsite early warning method for the Taiwan early warning system, *Bull. Seismol. Soc. Am.* **95**, 347–353, doi: [10.1785/0120040097](https://doi.org/10.1785/0120040097).
- Wu, Y. M., and T. L. Lin (2013). A test of earthquake early warning system using low cost accelerometer in Hualien, Taiwan, in *Early Warning for Geological Disasters—Scientific Methods and Current Practice*, F. Wenzel and J. Zschau (Editors), Springer, Berlin, Germany, 253–263.
- Wu, Y. M., and T. L. Teng (2002). A virtual subnetwork approach to earthquake early warning, *Bull. Seismol. Soc. Am.* **92**, 2008–2018, doi: [10.1785/0120010217](https://doi.org/10.1785/0120010217).
- Wu, Y. M., R. M. Allen, and C. F. Wu (2005). Revised M_L determination for crustal earthquake in Taiwan, *Bull. Seismol. Soc. Am.* **97**, 2517–2524, doi: [10.1785/0120050043](https://doi.org/10.1785/0120050043).
- Wu, Y. M., C. H. Chang, L. Zhao, T. L. Teng, and M. Nakamura (2008). A comprehensive relocation of earthquakes in Taiwan from 1991 to 2005, *Bull. Seismol. Soc. Am.* **98**, 1471–1481, doi: [10.1785/0120070166](https://doi.org/10.1785/0120070166).
- Wu, Y.-M., D.-Y. Chen, T.-L. Lin, C.-Y. Hsieh, T.-L. Chin, W.-Y. Chang, W.-S. Li, and S.-H. Ker (2013). A high-density seismic network for earthquake early warning in Taiwan based on low cost sensors, *Seismol. Res. Lett.* **84**, no. 6, 1048–1054, doi: [10.1785/0220130085](https://doi.org/10.1785/0220130085).
- Wu, Y. M., W. T. Liang, H. Mittal, W. A. Chao, C. H. Lin, B. S. Huang, and C. M. Lin (2016). Performance of a low-cost earthquake early warning system (P -alert) during the 2016 M_L 6.4 Meinong (Taiwan) earthquake, *Seismol. Res. Lett.* **87**, no. 5, 1050–1059, doi: [10.1785/0220160058](https://doi.org/10.1785/0220160058).
- Wu, Y. M., T. C. Shin, and Y. B. Tsai (1998). Quick and reliable determination of magnitude for seismic early warning, *Bull. Seismol. Soc. Am.* **88**, 1254–1259.

Department of Geosciences
National Taiwan University
No. 1, Sec. 4, Roosevelt Road
Taipei 10617, Taiwan
tingchunguang@gmail.com
yihmin.wu@gmail.com
b98204032@gmail.com

Manuscript received 30 March 2017;

Published Online 3 April 2018